Heliyon 8 (2022) e09420

Contents lists available at ScienceDirect

Heliyon

journal homepage: www.cell.com/heliyon

Research article

The role of organic acid metabolites in geo-energy pipeline corrosion in a sulfate reducing bacteria environment

Makungu Madirisha [a,b,*], Robert Hack [a], Freek van der Meer [a]

[a] Department of Applied Earth Sciences, Faculty of Geo-Information Science and Earth Observation (ITC), University of Twente, P.O. Box 217, 7500 AE, Enschede, the Netherlands

[b] Chemistry Department, College of Natural and Applied Sciences (CoNAS), University of Dar es Salaam, P. O. Box 35061, Dar es Salaam, Tanzania

ARTICLE INFO

Keywords:
Organic acid metabolites
Corrosion
Sulfate reducing bacteria
Geo-energy pipeline

ABSTRACT

The dominant factors in Microbial Influenced Corrosion (MIC) are hard to determine because normally several individual species and their metabolites are involved, and, moreover, different metabolites may cause opposing effects. To address this problem, the effects of individual metabolites from different species should be elucidated when at the same time other metabolites are held constant. In this study, the role is investigated of simulated organic acid metabolites, namely, acetic and L–ascorbic acids, on corrosion of geo-energy pipelines (carbon steel) in a simulated Sulfate Reducing Bacteria (SRB) environment. The SRB environment is simulated using a calcium alginate biofilm, abiotic sulfide, CO_2, and NaCl brine. The electrochemical results show that both simulated organic acid metabolites accelerate corrosion in a simulated SRB environment. The results are further supported by electrochemical weight losses, kinetic corrosion activation parameters, multiple linear regression, ICP-OES, pH, and XRD. However, a comparison of electrochemical results with those published in the literature for a simulated SRB environment without acetic or L-ascorbic acid under similar experimental conditions shows that the presence of acetic in this study results in lower corrosion current densities while in presence of L-ascorbic acid results into higher corrosion current densities. This implies that acetic and L-ascorbic acids inhibit and accelerate corrosion, respectively. In addition, the results highlight that H_2S is a key role of corrosion in the presence of organic acid. The results of this study are important new and novel information on the role of acetic and L-ascorbic acids in corrosion of geo-energy pipelines in the SRB environment.

1. Introduction

Water in geological reservoirs and installations for oil, gas, and non-volcanic geothermal energy normally contains NaCl and minor other elements such as Ca^{2+}, Mg^{2+}, SO_4^{2-}, I^-, Br^-, CO_3^{2-}, and HCO_3^- (Dresel and Rose, 2010; Magot et al., 1997, 2000; Muramatsu et al., 2000; Nogara and Zarrouk, 2018). This mix is commonly denoted "brine". According to Magot et al. (1997), the presence of SO_4^{2-} and CO_3^{2-} in water is evidence for the existence of microbes with metabolic processes, e.g. sulfate reduction and acetogenesis. Water is a suitable medium to support the growth of microbes and dissolve metabolic byproducts. The dissolved metabolic byproducts in water result in the formation of a corrosive solution that in conjoint interactions with chloride ions limit the application of metallic materials in the oil, gas, and geothermal industry (Ibrahim et al., 2018; Kiani Khouzani et al., 2019; Provoost et al., 2018).

Corrosion of metallic materials is a serious multibillion-dollar problem in the oil, gas, and geothermal industry (geo-energy) as corrosion reduces mechanical properties leading to loss of materials, and ultimately failure (Abadeh and Javidi, 2019; Ahmad, 2006; Cramer and Covino, 2003; Li and Ning, 2019; Popoola et al., 2013; Reinecker et al., 2019; Wang et al., 2019). Metallic materials used in the geo-energy industry are susceptible to different forms of corrosion, such as general and localized corrosion, and pitting (Dariva and Galio, 2014; Streicher, 2011). Localized corrosion mainly caused by biotic factors, also known as Microbial Influenced Corrosion (MIC) is a major cause of pipeline leakage (Alabbas and Mishra, 2013; Clarke and Aguilera, 2001; Li et al., 2018). MIC is a

* Corresponding author.
E-mail addresses: m.m.madirisha@utwente.nl, makungumarco@udsm.ac.tz (M. Madirisha).

https://doi.org/10.1016/j.heliyon.2022.e09420
Received 23 November 2021; Received in revised form 15 January 2022; Accepted 10 May 2022

problematic type of corrosion because MIC is difficult to identify compared to abiotic corrosion. Further, it does not have a specific form (Little et al., 2020; Riskin and Khentov, 2019). Further, the type and capability of microbial metabolites that are causing corrosion are uncertain too (Little et al., 2006). The most dominant and troublesome species of MIC are Sulfate Reducing Bacteria (SRB) that exist in complex microbial communities (Audiffrin et al., 2003; Hussain et al., 2016; Plugge et al., 2011; Wolf et al., 2016).

2. Microbial influenced corrosion due to Sulfate Reducing Bacteria

Sulfate reducing bacteria (SRB) are ubiquitous anaerobes which are the most studied corrosive microbes in the geo-energy industry because sulfate ions are frequently present (Jia et al., 2017). SRB require an electron donor and acceptor to provide energy for their metabolism. Low-molecular-weight organic compounds are used as electron donors while sulfate ions are used as the terminal electron acceptor (reduced to HS^-). According to Gu et al. (2019), SRB consume also elemental iron as an electron donor when there is a lack of low-molecular-weight organic compounds (carbon source). In SRB corrosion, bacterial biofilms shuttle electrons across the cell wall from extracellular iron oxidation to the cytoplasm, where sulfate reduction occurs under biocatalysis (Gu et al., 2019; Li et al., 2018). Extracellular electron transfer (EET) is the term for electron transfer across cell walls (Jia et al., 2018; Li et al., 2015). As a result, EET-MIC is the first type of microbial influenced corrosion (MIC). During EET-MIC, electrons can be transferred directly or by electron shuttles. Some SRBs are said to have outer-membrane cytochromes (OMCs) that exchange electrons directly with electron shuttles in the latter situation (Li et al., 2019; Wang et al., 2020). Secreted metabolites such as H_2S, CO_2, and organic acids are also reported to cause corrosion which is known as metabolite MIC (M-MIC), and this type of corrosion is the central focus of this paper.

3. Influence of organic acid metabolites on corrosion

The distribution of microbes in a microbial community is not homogeneous (Almela et al., 2021; Davis and Isberg, 2016). Different interacting species of microbes are known to be present producing different metabolites which in turn result in metabolic heterogeneity within bacterial communities (Kim et al., 2015; Wong et al., 2021). Different microbial species can share a living space, for example, SRB with methanogens, SRB with acetogenic, and SRB with fermentative bacteria (acid producing bacteria). SRB and methanogens compete for acetate and H_2 while SRB and acetogenic compete for propionate, butyrate, and ethanol. SRB depend on fermentative bacteria (Figure 1) which cleave and ferment the complex organic matter to low-molecular-weight organic compounds. SRB do not metabolize complex organic compounds, such as those included as substrates in the test medium, instead metabolize short chain organic acids (low-molecular-weight organic acids). Fermentative bacteria produce a variety of low molecular weight organic compounds, and these include organic acids (acetic, L-ascorbic, gluconic, glucuronic, formic, peroxides and oxalic, oxalacetic, butyric, succinic, propionic, fumaric, citric, malic, and glyoxylic acid, kojic, phenylacetic, indolylacetic, dihydroxydibenzenecarboxylic, glutaconic and 4-hydroxymandelic acids), ketones, and alcohols (ethanol, propanol, and butanol) (Bao et al., 2012; Kushkevych et al., 2021; Lugauskas et al., 2009; Naranjo et al., 2015; Sand and Gehrke, 2003; Tran et al., 2021).

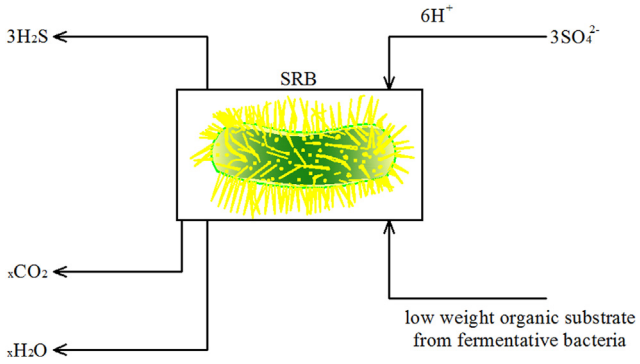

Figure 1. Dependency of SRB on fermentative bacteria for nutrition.

In the absence or low concentration of an external electron acceptor, fermentative microbes such as acid producing bacteria and SRB strains oxidize an organic carbon (e.g aromatic and aliphatic hydrocarbons in oil and gas) and produce energy through substrate-level phosphorylation (Xu et al., 2016). Organic acids are the main products also in this type of anaerobic fermentation. The combinations of different metabolites in a microbial community are likely to have a particular kinetic effect on corrosion that is specific to the combination of metabolites (Videla and Herrera, 2009). For example, organic acids are reported to react with materials of natural and/or synthetic origin causing swelling, total or partial dissolution, and, finally, deterioration (Caneva et al., 2008). Organic acids undergo reactions with materials by either the action of protons or chelation with metal ions and therefore promote corrosion by destroying the oxide layer formed on the material surface (Caneva et al., 2008). Despite the direct role of organic acids on materials being commonly known, their role in combination with SRB environment is still unclear. The presence of organic acid metabolites in SRB environment e.g organic acid from fermentative bacteria might result in an aqueous medium with unique corrosion kinetics (Bao et al., 2012; Bonis and Crolet, 1989; Crolet and Bonis, 1983). A study on organic acid metabolites in combination with a SRB environment is important to establish the possible interactions of SRB with other chemical species and with the metals in installations for oil, gas and non-volcanic geothermal energy.

The present study aims to investigate the role of organic acid metabolites, namely acetic and L-ascorbic acid (0.2 and 1.0 mM) on corrosion of geo-energy pipelines made from carbon steel, in a simulated SRB environment. The carbon steel corrosion study is simulated in an electrochemical cell with different temperatures (30, 45, and 60 °C) and exposure times (60 and 120 min). Electrochemical techniques are used to monitor the corrosion parameters and the results obtained are supported further by kinetic corrosion of activation, multiple linear regression of corrosion current densities, Inductively Coupled Plasma - Optical Emission Spectrometry (ICP-OES), pH, and X-Ray Diffraction (XRD).

4. Materials and methods

4.1. Preparation of test coupons

The electrochemical cell's carbon steel working electrodes (also known as "test coupons") are prepared from carbon steel used in gas pipes (API 5L X70M HFW), which is provided by the Tanzania Petroleum Development Corporation. Table 1 shows the chemical composition of the carbon steel test coupon. The test coupons are round disks with a radius of 7 mm and a thickness of 1.5 mm. Each one is polished with 100, 200, 400, 600, 800, and 1000 grit silicon carbide papers, in order of decreasing particle size. The test coupons are then rinsed with distilled water and sonicated in ethanol for about 15 min before being rinsed with acetone and dried. After air drying, the test coupons are weighed on an electronic analytical balance.

Table 1. Chemical composition of carbon steel API 5L X70M HFW (wt%).

Fe	C	Si	Mn	P	S	V	Nb	Ti
97.39	0.17	0.45	1.75	0.020	0.010	0.10	0.050	0.060

4.2. Preparation of biofilm and organic acid metabolites

A mimicked biofilm is prepared in this study because biofilms are often present in bacteria communities (Alabbas and Mishra, 2013; Blackwood, 2018; Parthipan et al., 2017; Zuo, 2007). Calcium alginate is used to model biofilm because it is comparable to the structure and properties of biofilm in real settings, as reported by numerous authors (Chang et al., 2010; Nassif et al., 2020). Furthermore, corrosion rates of 0.25–1.6 mm/year have been reported when calcium alginate is combined with SRB metabolites, which are close to previous corrosion rates obtained in SRB trials (0.20–1.2 mm/year). This means that the simulated H_2S, CO_2, and biofilm for corrosion investigations are indicative of the SRB media (Madirisha et al., 2022).

In preparation of a simulated biofilm, a fine strand of nylon is used to evenly spread sodium alginate (Figure 2a) solution over the entire surface of the prepared test coupons. After that, 0.1 mL of 0.004 M aqueous $CaCl_2$ is applied to the surface and left for 15 min to allow the reaction to occur. The test coupons are washed with 10 mL of distilled water to eliminate any unreacted Na-alginate. Finally, the test coupons are air-dried. Furthermore, organic acids: acetic and L-ascorbic (Figure 2b,c) are prepared at the concentration of 0.2 and 1.0 mM. The pH of 2.6 at the concentration of 0.2 and 1.0 mM acetic or L-ascorbic acid is prepared. The type and concentration of acids are chosen to represent organic acids produced by non-SRB.

4.3. Electrochemical cell

The electrochemical tests are carried out in a three-electrode electrochemical cell with a Metrohm PGSTAT204/AUT50663 potentiostat/galvanostat (Autolab B.V., Amsterdam, The Netherlands). The program used is Metrohm's NOVA version 1.11.2 (Autolab B.V., Amsterdam, The Netherlands). In addition, an electrochemical cell is connected to a thermostat-water bath, a pH meter, and a CO2 gas cylinder (Figure 3). Working, auxiliary, and reference electrodes are made of carbon steel coated with biofilm, platinum, and saturated silver-silver chloride (Ag/AgCl) in 3.0 M KCl, respectively. A 3.0 weight percent NaCl solution is used to mimic brine in oil, gas, and non-volcanic geothermal energy installations. The electrochemical cell's solution of simulated brine and organic acid metabolites is purged with CO_2 at a rate of around 150 mL/min to establish an anaerobic environment while also serving as a product of SRB dissimilatory sulfate reduction. The purging process begins 30 min before the experiment and continues until the experiment is completed. The test matrix (Table 2) is designed so that the total volume of the solution in the electrochemical cell is 500 mL, with a volume ratio of 487: 10: 3 for 3.0 weight percent NaCl solution (to represent brine), organic acid metabolites, and 0.4 M $Na_2S.xH_2O$ (to mimic H_2S), respectively. Corrosion tests are carried out at temperatures of 30, 45, and 60 °C, with exposure durations of 60 and 120 min.

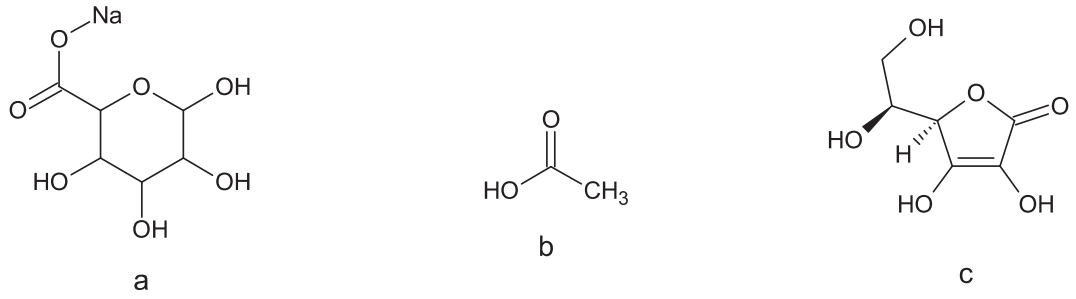

Figure 2. Structure of sodium alginate(a), acetic acid (b), and L-ascorbic (c).

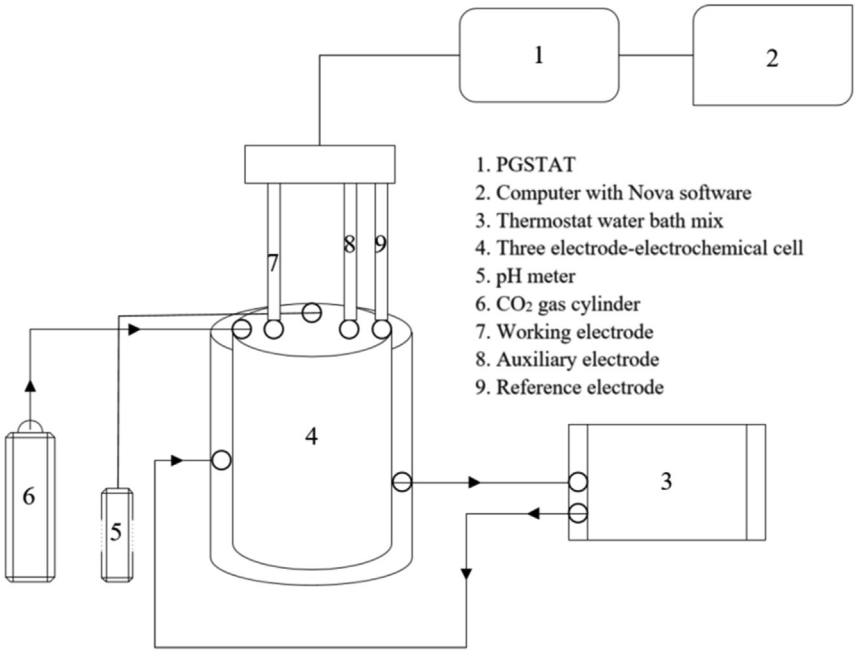

Figure 3. Schematic diagram of the set-up for carbon steel corrosion tests (Madirisha et al., 2022). The Copyright Permission of this Figure has been granted by Elsevier and Copyright Clearance Center.

Table 2. Experiments for the investigation of the role of organic acid metabolites on the corrosion of carbon steel.

Acid	Experiment	Temperature (°C)	Concentration of acid (mM)	Time (min)
Acetic acid	1, 2, 3	30, 45, 60	0.2	60
	4, 5, 6	30, 45, 60	1.0	60
	7, 8, 9	30, 45, 60	0.2	120
	10, 11,12	30, 45, 60	1.0	120
L-Ascorbic acid	13, 14, 15	30, 45, 60	0.2	60
	16, 17, 18	30, 45, 60	1.0	60
	19, 20, 21	30, 45, 60	0.2	120
	22, 23, 24	30, 45, 60	1.0	120

All tests are carried out twice. Furthermore, the pH of the solution is monitored during the tests at the start, as well as every 60 and 120 min. Initial pH is the pH recorded at the start of the test, whereas final pH is the pH recorded after 60 and 120 min. After each test, the test coupon is taken out of the cell and placed in a desiccator for further analysis.

4.4. Methods

4.4.1. Electrochemical corrosion measurements

The electrochemical corrosion measurements by Electrochemical Impedance Spectroscopy (EIS) and by PotentioDynamic Polarization (PDP) are done in the electrochemical cell after 60 and 120 min. The EIS is carried out in a frequency range of 0.5 mHz–10 kHz with a perturbation amplitude of 10 mV. The measurements are all performed at the open circuit potential and are taken after 60 min and 120 min exposure time. Furthermore, the electrochemical circle fitting -analysis on EIS data is done using the NOVA software to generate the polarization resistance (R_p), solution resistance (R_s), and constant phase elements (CPE): pseudo-capacitance/admittance (Y_o), and phase shift/index (n).

The PDP is measured by sweeping the potential at a rate of 10 $mVmin^{-1}$ in the range of -200 to 200 mV vs Ag/AgCl reference electrode, i.e cathodically and anodically from open circuit potential. The Tafel slopes (b_a and b_c) are determined after a stable open circuit potential is achieved by extrapolating the linear Tafel regions to the corrosion potential (E_{corr}). All polarization measurements are performed after the electrochemical impedance measurements.

4.4.2. Gravimetric analysis

Gravimetric analysis is done by conversion of the obtained corrosion current density to the more comprehensive electrochemical weight loss. This follows Faraday's law (Eq. (1)) (Apostolopoulos et al., 2013; Munoz et al., 2007; Sanchez et al., 2017):

$$\Delta W(g) = \frac{P\int Idt}{F} \tag{1}$$

where P is the equivalent weight of iron with a valence of 2; I is corrosion current density; t = time; the integral $\int Idt$ corresponds to the area under the curve obtained in the electrochemical measurements (I_{corr} - time curve); and F is the Faraday constant of about 9.65×10^4 C mol^{-1}.

4.4.3. Kinetic parameters of activation corrosion

The Arrhenius Eq. (2) and transition state Eq. (3) are used to determine the kinetic parameters of activation corrosion namely, apparent activation corrosion energy (E_{act}), enthalpy of activation (ΔH_{act}), and entropy of activation (ΔS_{act}). The E_{act}, ΔH_{act}, and ΔS_{act} have a direct influence on the corrosion current densities of the material (Go et al., 2020; Khadom et al., 2009).

$$\log I_{corr} = \log A - \frac{E_{act}}{2.303RT} \tag{2}$$

$$I_{corr} = \frac{RT}{Nh} e^{\frac{\Delta S_{act}}{R}} e^{-\frac{\Delta H_{act}}{RT}} \tag{3}$$

A is the pre-exponential factor, R is the universal gas constant of 8.314 J/(mol·K), T is the testing temperature (K), N is Avogadro's number, h is Plank's constant.

4.4.4. Characterization of the dissolved metal ions in solution

The ICP-OES (PerkinElmer 8300DV) is used to quantify Fe, Si, and Mn ions dissolved in the solution after every test. Before the ICP-OES analysis, stepwise dilution of a multi-element (1000 mg/L) ICP standard solution (Merck) to make working standard solutions is performed. The prepared solutions are filled into ICP-OES tubes and introduced into the autosampler of the ICP-OES machine. Calibration of blanks (DW and brine) and the prepared working standard solution are performed. For standard solution, calibration is performed ranging from low to high concentration. Thereafter, both blank samples and the supernatant (samples collected after electrochemical measurements) are inserted into the autosampler ready for analysis. To obtain the corrected ICP-OES results, the ICP-OES results of supernatant samples are subtracted with the ICP-OES results of blanks of distilled water and brine. The corrected ICP-OES results (mg/L) are finally normalized to the weight of the working electrode (g), working electrode exposed geometrical surface area (cm^2), and the total solution volume (L) in the electrochemical cell. The normalized results are expressed in $\mu g/g.cm^2$.

4.4.5. Inferential statistics

Inferential statistics is the branch of statistics allowing to make predictions ("inferences") from the data collected. Regression analysis is chosen to ascertain the extent of the relationship between the outcome variable (dependent variable) and predictor variables (independent variables). The regression analysis is performed by using the IBM SPSS statistics 27 software. Multiple linear regression is performed on corrosion current density (I_{corr}) as a function of temperature, exposure time, the concentration of acids, and pH of the solution.

4.4.6. Characterization of corrosion products

The characterization of the corrosion products on the corroded test coupons is performed using XRD (Bruker D2 phaser) with CuKα radiation, LYNXEYE detector, and corundum as an ideal internal standard. To collect the diffractogram, the XRD machine is set to operate at 1.54184 Å, 10 mA, 30 kV, and 6° to 80°in the 2θ range with the step size of 0.012° and integration time of 0.1s. In addition, a standard divergence slit of 0.6 mm to control the illuminated area, and a detector slit of 8 mm where X rays are refocused are used. The DIFFRA.EVA software is used for the identification of the obtained diffractograms. Each corroded test coupon was measured for 24 h. Furthermore, fresh test coupon was used as a reference.

5. Results and discussion

5.1. PotentioDynamic polarization

The electrochemical results of the PDP measurements determining the influence of acetic acid (0.2 and 1.0 mM) are shown in Table 3. The PDP results show that the corrosion potentials (E_{corr}) at exposure times of 60 and 120 min are less negative than the standard potential (E) of iron which is -680 mV (Standard Calomel Electrode (SCE)). A negative over potential implies that the reduction reaction (cathodic reaction) dominates the corrosion process. The possible cathodic chemical equations are Eqs. (4), (5), and (6):

Table 3. Electrochemical parameters (PDP) for test coupons in brine solution as function of time, acetic acid and temperature.

t (min)	[Acetic] (mM)	T (°C)	E_{corr} (mV, Ag/AgCl)	I_{corr} (mAcm^{-2})	b_a (mVdec^{-1})	b_c (mVdec^{-1})	R_p (Ω)
60	0.2	30	-668 ± 2	0.07 ± 0.00	241 ± 14	61 ± 3	286 ± 3
		45	-670 ± 1	0.08 ± 0.00	220 ± 11	60 ± 1	275 ± 1
		60	-672 ± 4	0.09 ± 0.00	192 ± 2	55 ± 1	273 ± 1
	1.0	30	-682 ± 1	0.12 ± 0.01	253 ± 17	66 ± 5	198 ± 4
		45	-684 ± 2	0.13 ± 0.01	235 ± 15	62 ± 2	192 ± 1
		60	-686 ± 1	0.14 ± 0.01	204 ± 2	56 ± 3	125 ± 1
120	0.2	30	-643 ± 1	0.06 ± 0.02	179 ± 8	62 ± 2	280 ± 3
		45	-666 ± 3	0.07 ± 0.01	166 ± 4	60 ± 1	275 ± 1
		60	-670 ± 3	0.08 ± 0.02	146 ± 10	63 ± 4	247 ± 5
	1.0	30	-680 ± 2	0.11 ± 0.00	248 ± 11	75 ± 10	213 ± 1
		45	-686 ± 1	0.13 ± 0.00	216 ± 1	72 ± 0	161 ± 1
		60	-692 ± 2	0.14 ± 0.00	196 ± 5	64 ± 2	113 ± 1

Table 4. Electrochemical parameters (PDP) for test coupons in brine solution as function of time, L-ascorbic acid and temperature.

t (min)	[L-ascorbic] (mM)	T (°C)	E_{corr} (mV, Ag/AgCl)	I_{corr} (mAcm^{-2})	b_a (mVdec^{-1})	b_c (mVdec^{-1})	R_p (Ω)
60	0.2	30	-681 ± 2	0.89 ± 0.00	136 ± 11	59 ± 3	528 ± 21
		45	-705 ± 1	1.17 ± 0.01	179 ± 4	59 ± 5	402 ± 27
		60	-708 ± 1	1.68 ± 0.00	341 ± 14	58 ± 8	380 ± 1
	1.0	30	-711 ± 1	1.88 ± 0.01	390 ± 42	87 ± 7	194 ± 1
		45	-713 ± 3	2.12 ± 0.00	431 ± 27	89 ± 4	182 ± 7
		60	-717 ± 2	2.77 ± 0.01	538 ± 82	96 ± 6	79 ± 1
120	0.2	30	-685 ± 1	0.97 ± 0.00	179 ± 4	54 ± 1	417 ± 4
		45	-707 ± 2	1.49 ± 0.00	229 ± 3	66 ± 6	364 ± 1
		60	-710 ± 1	1.84 ± 0.00	239 ± 4	67 ± 1	312 ± 1
	1.0	30	-715 ± 2	2.22 ± 0.00	399 ± 70	85 ± 15	163 ± 2
		45	-721 ± 1	2.94 ± 0.00	413 ± 81	88 ± 15	118 ± 1
		60	-748 ± 2	3.32 ± 0.00	576 ± 94	130 ± 17	72 ± 1

$$2H_2S + 2e^- \rightarrow 2HS^- + H_2 \quad (4)$$

$$2HAc + 2e- \rightarrow H_2 + 2Ac^- \quad (5)$$

$$2H_2CO_3 + 2e^- \rightarrow H_2 + 2HCO_3^- \quad (6)$$

Furthermore, an increase in corrosion current densities and Tafel slopes is observed when temperature increases in the presence of either 0.2 or 1.0 mM. This increase in corrosion current with increasing temperature is likely due to either a rapid increase in the amount of hydrogen species as a result of an increase in the extent of chemisorption of acetic acid on the surface of test coupons as described by the chemical Eqs. (7) and (8) (Amri et al., 2011; Singh and Gupta, 2000) or dissociation of H_2S according to Eq. (2). Other authors report that such an increase in corrosion current as temperature increases is likely due to direct acetic acid reduction during the corrosion process, Eq. (5) (Kahyarian et al., 2017).

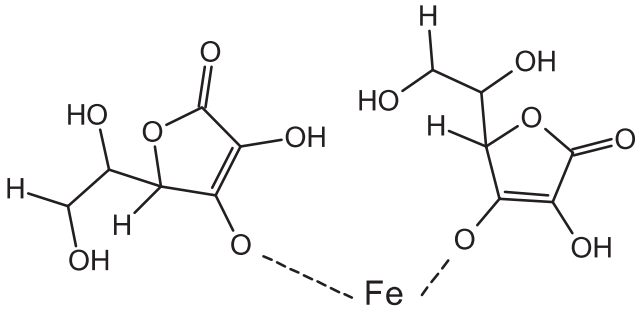

Figure 4. Formation of chelating complex between Fe^{2+} and L- Ascorbic acid.

$$HAc_{(ad)} \rightleftharpoons H^+ + Ac^- \rightleftharpoons H_{(ad)} + Ac^- \quad (7)$$

$$H_{(ad)} + H^+ \rightleftharpoons H_2 \quad (8)$$

On the other hand, an increase in corrosion current densities when the concentration of acetic acid increases can be explained by Le-Chatelier's Principle. Taking into account Eq. (7), an increase in the

Table 5. Polarization resistance, solution resistance, and CPEs for test coupons in brine solution experiments as a function of time, acetic acid, and temperature.

t (min)	[Acetic] (mM)	T (°C)	R_p (Ω)	R_s (Ω)	CPEs	
					Y_o (x10^{-2} μF)	n
60	0.2	30	22.60 ± 0.11	2.24 ± 0.05	1.799	1.000
		45	15.55 ± 0.01	0.98 ± 0.00	2.201	1.000
		60	14.24 ± 0.12	0.77 ± 0.06	2.493	1.000
	1.0	30	17.03 ± 0.21	0.82 ± 0.14	2.362	1.000
		45	15.40 ± 0.06	0.58 ± 0.08	2.395	1.000
		60	12.62 ± 0.42	0.21 ± 0.06	2.522	1.000
120	0.2	30	15.74 ± 0.63	0.46 ± 0.15	2.557	1.000
		45	13.63 ± 0.51	0.32 ± 0.08	2.519	1.000
		60	13.18 ± 0.01	0.31 ± 0.06	2.616	1.000
	1.0	30	13.62 ± 0.54	0.40 ± 0.02	2.225	1.000
		45	12.22 ± 0.01	0.32 ± 0.00	2.243	1.000
		60	09.03 ± 0.13	0.29 ± 0.08	2.444	1.000

Table 6. Polarization resistances, solution resistances, and CPEs for test coupons in brine solution experiments as a function of time, L-ascorbic acid, and temperature.

t (min)	[L-ascorbic] (mM)	T (°C)	R_p (Ω)	R_s (Ω)	CPEs	
					Y_o (x10^{-2} μF)	n
60	0.2	30	20.18 ± 1.28	1.58 ± 0.15	1.953	1.000
		45	16.49 ± 1.29	0.77 ± 0.02	2.096	1.000
		60	12.84 ± 1.65	0.44 ± 0.07	2.330	1.000
	1.0	30	16.45 ± 0.13	0.32 ± 0.06	1.954	1.000
		45	14.40 ± 0.19	0.18 ± 0.08	1.965	1.000
		60	12.78 ± 0.09	0.07 ± 0.06	2.372	1.000
120	0.2	30	18.41 ± 1.33	0.33 ± 0.15	1.751	1.000
		45	14.92 ± 1.11	0.11 ± 0.08	1.954	1.000
		60	11.96 ± 1.99	0.09 ± 0.06	2.372	1.000
	1.0	30	13.65 ± 0.07	0.90 ± 0.04	1.772	1.000
		45	11.67 ± 0.08	0.88 ± 0.05	2.065	1.000
		60	09.78 ± 0.09	0.67 ± 0.06	2.603	1.000

concentration of acetic acid favours the right-hand side reaction and hence rapidly favours the cathodic reaction. An increase in corrosion current upon an increase in acetic concentration is likely also linked to the absence of dimer and polymer formation associated with acetic acid. The lack of dimer and polymer formation is likely to boost the ions' mobility (hydrogen ions and anionic conjugate base) (Singh and Mukherjee, 2010). However, comparison on the corrosion current densities in the presence of acetic acid in this study are two times lower than without acetic acid under similar experimental conditions reported in Madirisha et al. (2022). In addition, a significant change in Tafel slope is observed. Lower corrosion current densities evidenced in the presence of acetic acid in a SRB environment implies an inhibitory effect occurring on the working electrode while the significant change in Tafel slopes indicates the change in species involved in the reaction. This research finding implies that acetic acid does not accelerate the corrosion process instead it triggers the localized attack of a metal surface. Furthermore, H_2S is the responsible species in accelerating corrosion. Acetic acid inhibits the cathodic hydrogen ion reduction reaction and the anodic iron dissolving reaction, which has a substantial impact on the corrosion process. When the temperature and concentration of acetic acid are increased, however, the inhibition is reduced. The uniqueness of this study is highlighted by the inhibitory effect of acetic acid in a simulated SRB.The inhibitory effect demonstrated by acetic acid in a simulated SRB setting highlights the novelty of this work.

Replacing acetic acid with L-ascorbic acid results in corrosion potentials greater than the standard potential (E) of iron (Table 4) which is -680 mV (SCE) which implies that the anodic reaction is dominant compared to the cathodic reaction. The possible anodic reaction involved is the dissolution of iron to ferrous ions given by Eq. (9) while the cathodic reactions are given by Eqs. (4), (6), and (10).

$$Fe \rightarrow Fe^{2+} + 2e^{-} \quad (9)$$

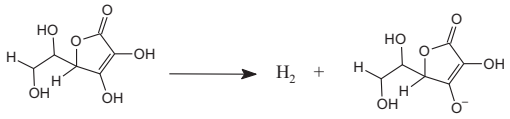

(10)

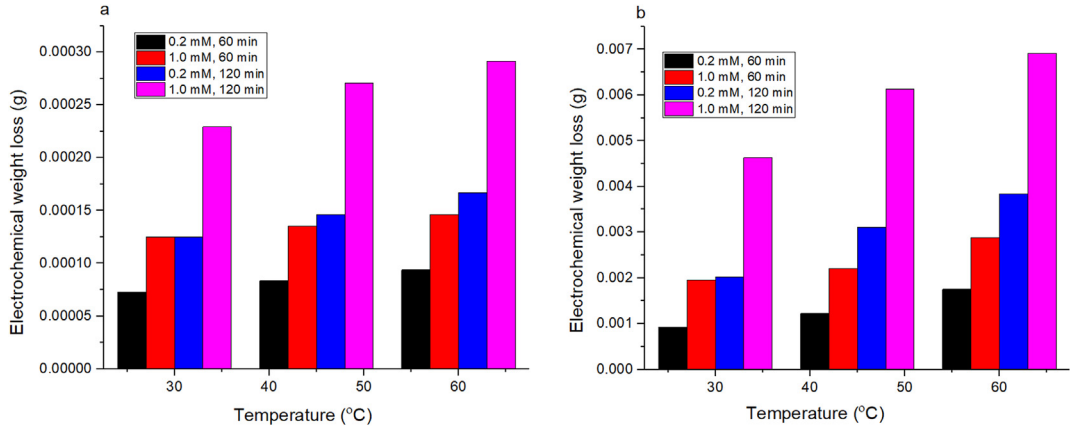

Figure 5. Electrochemical weight loss of test coupons as a function of the concentration of acids, exposure time, and temperature: (a) acetic acid (b) L-ascorbic acid.

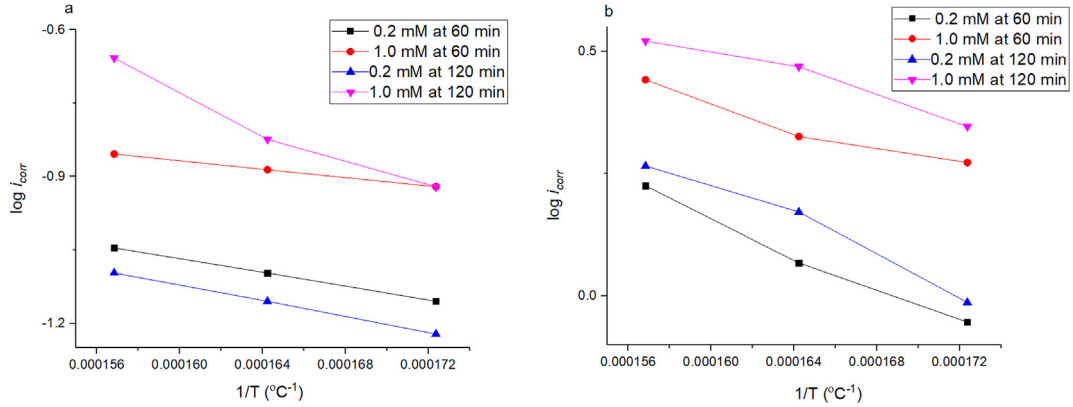

Figure 6. Plot of log i_{corr} vs 1/T as a function of the concentration of acids and exposure time: (a) acetic acid (b) L-ascorbic ascorbic.

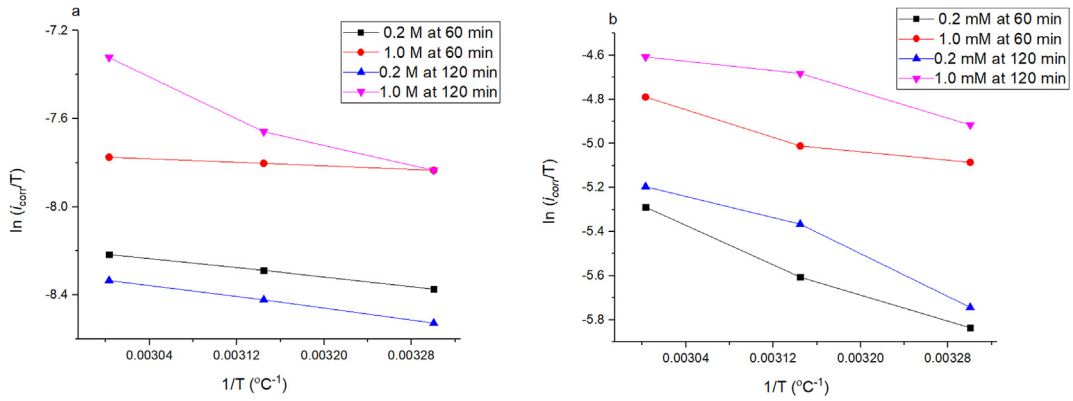

Figure 7. Plot of 1/T vs ln (i_{corr}/T) as a function of concentration of acids and exposure time: (a) acetic acid (b) L-ascorbic ascorbic.

Table 7. The apparent activation corrosion energy (E_{act}), enthalpy of activation (Δ H_{act}) and entropy of activation (Δ S_{act}) as the function of temperature and corrosion current density (i_{corr}).

Acid	Conc. (mM)	Time (min)	E_{act} (kJ/mol)	Δ H_{act} (kJ)	Δ S_{act} (kJ/K)
Acetic	0.2	60	7.03	4.39	-0.26
	1.0		4.31	1.67	-0.27
	0.2	120	8.05	5.41	-0.26
	1.0		6.78	4.14	-0.27
L-ascorbic	0.2	60	17.89	15.25	-0.21
	1.0		10.84	8.28	-0.22
	0.2	120	18.03	15.39	-0.21
	1.0		11.33	8.69	-0.22

In the presence of L-ascorbic acid, the I_{corr}, E_{corr}, and Tafel slopes increase while R_p decreases when temperature increases. Comparing the corrosion current densities with those reported in a SRB environment without L-ascorbic acid under similar experimental conditions in Madirisha et al. (2022), the corrosion current densities are approximately two times higher implying higher corrosion rates. To elaborate, corrosion experiments with L-ascorbic acid alone have shown the acid to serve as the corrosion inhibitor for corrosive ions (Chidiebere et al., 2015; Fuchs-Godec et al., 2013; Hong et al., 2016). However, this increase in corrosion current densities observed under a SRB environment is likely associated with the formation of a chelating complex of high solubility that easily forms with Fe^{2+} (Figure 4). The increase in corrosion current densities in the presence of either 0.2 or 1.0 mM L-ascorbic acid under a simulated SRB environment is not found in the literature and therefore highlights the novelty of this research.

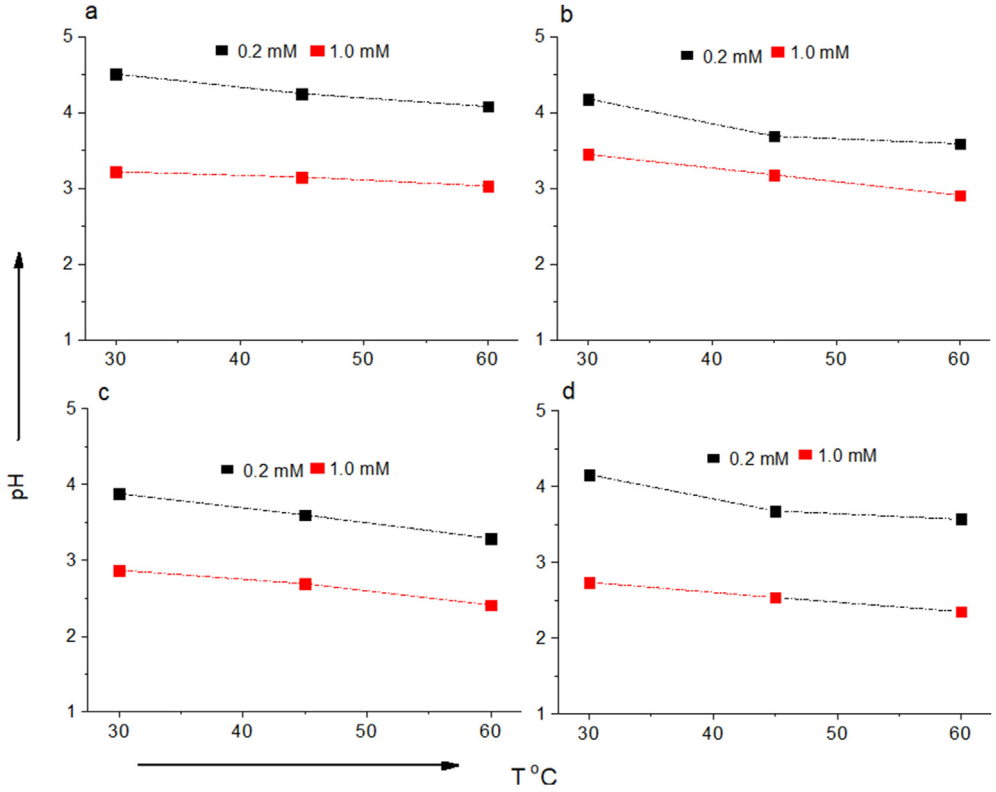

Figure 8. Final pH of the brine solution with organic acid metabolites as a function of time and temperature: (a) Acetic acid, 60 min (b) Acetic acid, 120 min (c) L-ascorbic acid, 60 min (d) L-ascorbic acid, 120 min.

5.2. Electrochemical Impedance Spectroscopy

The electrochemical results of the EIS measurements determining the influence of acetic acid (0.2 and 1.0 mM) are shown in Table 5. The increase in temperature and concentration of acetic acid shown in the EIS results in a decrease of R_p and R_s, and an increase of Y_o. The decrease in resistances (R_p and R_s) implies an increase in corrosion current densities. Moreover, the conversion of Y_o data into equivalent capacitance (C) which is governed by Eq. (11) shows that when $n = 1$ in Table 5, the pseudo capacitance (Y_o) is equal to equivalent capacitance (C_{dl}) and thus the CPEs are equivalent to pure capacitors. If $Y_o = C_{dl}$, the trend demonstrated by Y_o is also similar to $C_{dl.}$ and their increase reflects an increase in corrosion rate. These results further support the PDP results.

$$C_{dl} = Y_o^{\frac{1}{n}} R_p^{\frac{1-n}{n}} \tag{11}$$

The EIS results for L-ascorbic acid show a drop in R_p and R_s when the concentration of L-ascorbic acid, and temperature are increased (Table 6). The drop in R_p and R_s further supports the PDP results that L-ascorbic acid increases corrosion instead of acting as the corrosion inhibitor as reported in the literature (Ferreira et al., 2004; Fuadi, 2019). This increase in corrosion rate is in agreement with the increase in Y_o since $n = 1$ based on Eq. (11).

5.3. Gravimetric results

The gravimetric results based on electrochemical weight loss of test coupons in acetic and L-ascorbic acids as computed using Eq. (1) are presented in Figure 5. The electrochemical weight loss for test coupons in either acetic or ascorbic acid shown in both Figures increase with an increase in temperature and concentration of the acid. This implies an increase in corrosion current densities. The electrochemical weight loss is maximum at 60 °C for 1.0 mM of acid and 120-exposure time and minimum at 30 °C for 0.2 mM of acid and 60-exposure time. In addition, the electrochemical weight loss in the presence of L-ascorbic acid is higher than in the presence of acetic acid which in turn implies higher corrosion. These observations are in agreement with the PDP and EIS results.

5.4. Kinetic parameters of activation corrosion

The apparent activation corrosion energy (E_{act}) is estimated from the linear regression plot shown in Figure 6 of Arrhenius equation (Eq. (2)). Further, the enthalpy of activation (ΔH_{act}) and entropy of activation (ΔS_{act}) are also estimated from the linear regression plot shown in Figure 7 of the transition state equation (Eq. (3)). The numerical results are shown in Table 7. The kinetic parameters of activation corrosion, i.e. E_{act} and ΔH_{act}, in the presence of either acetic or ascorbic acid decrease with an increase in acid concentration. This implies an increase in corrosion

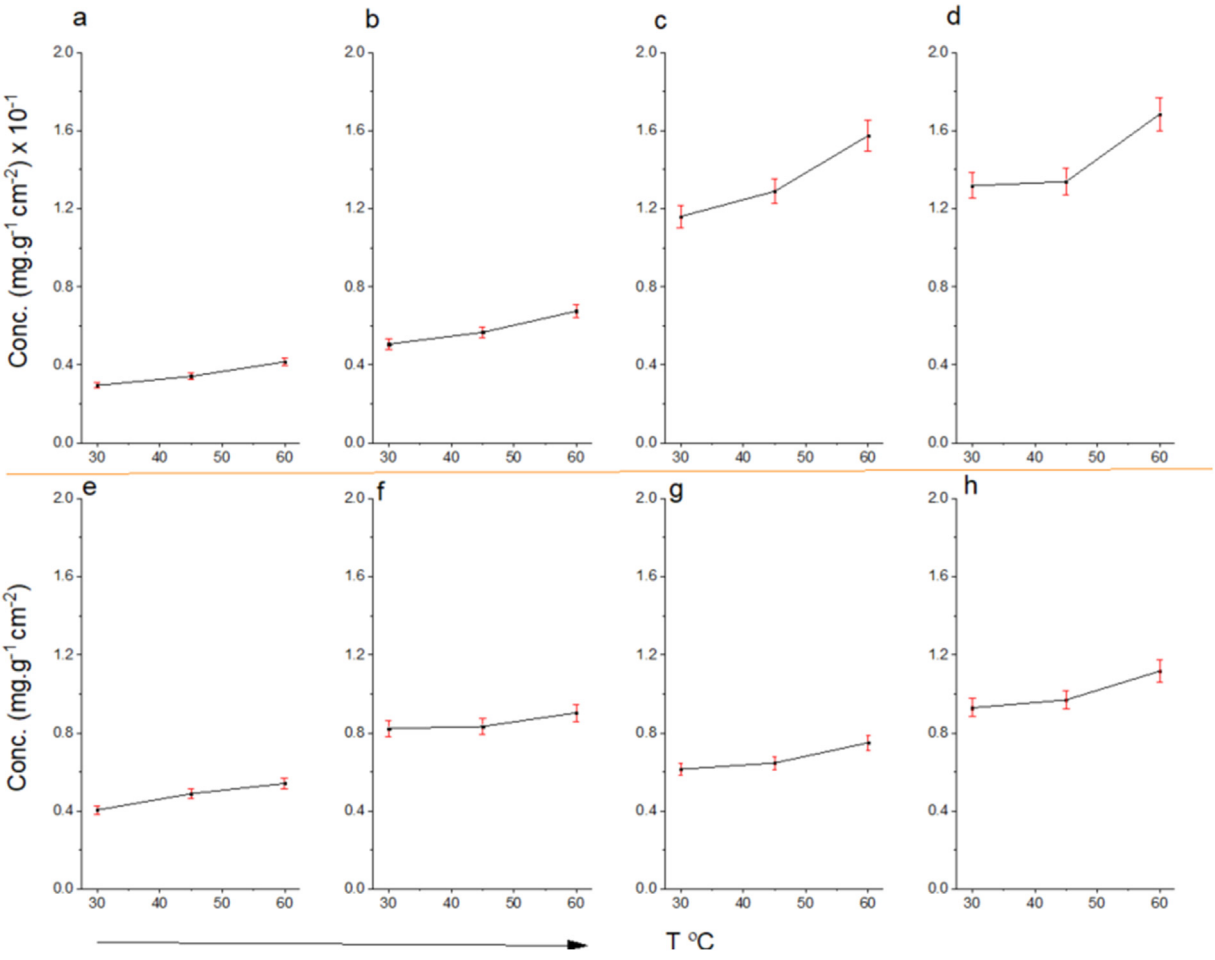

Figure 9. Dissolved cations (Fe, Si, and Mn) in a brine solution with organic acid metabolites as a function of time and temperature: (a) Acetic acid, 60 min and 0.2 mM (b) Acetic acid, 60 min and 1.0 mM (c) Acetic acid, 120 min and 0.2 mM (d) Acetic acid, 120 min, and 1.0 mM (e) L-ascorbic acid, 60 min and 0.2 mM (f) L-ascorbic acid, 60 min and 1.0 mM (g) L-ascorbic acid, 120 min and 0.2 mM (h) L-ascorbic acid, 120 min, and 1.0 mM.

Table 8. Corrosion current density, temperature, exposure time, the concentration of acids, and pH of the solution.

Acid	I_{corr}	T (°C)	Time (min)	Conc. (mM)	pH
Acetic	0.07	30	60	0.2	3.35
	0.08	45	60	0.2	3.01
	0.09	60	60	0.2	2.96
	0.12	30	60	1	2.68
	0.13	45	60	1	2.63
	0.14	60	60	1	2.48
	0.06	30	120	0.2	3.33
	0.07	45	120	0.2	2.99
	0.08	60	120	0.2	2.94
	0.11	30	120	1	2.71
	0.13	45	120	1	2.61
	0.14	60	120	1	2.54
L-ascorbic	0.89	30	60	0.2	2.84
	1.17	45	60	0.2	2.66
	1.68	60	60	0.2	2.41
	1.88	30	60	1	2.47
	2.12	45	60	1	2.27
	2.77	60	60	1	2.22
	0.97	30	120	0.2	2.93
	1.49	45	120	0.2	2.65
	1.84	60	120	0.2	2.46
	2.22	30	120	1	2.54
	2.94	45	120	1	2.31
	3.32	60	120	1	2,.24

Table 9. R^2, p and coefficient values of prediction of corrosion current density (i_{corr}) as a function of temperature, exposure time, the concentration of acids, and pH of the solution.

Acid	R^2	p	Model equation
Acetic	0.992	0.000	i_{corr} (acetic) = 0.001T + 0.000t + 0.075C + 0.014pH - 0.014
L-ascorbic	0.970	0.000	i_{corr} (L-ascorbic) = 0.033T + 0.006t + 1.602C + 0.254pH - 1.711

Notes: R^2: coefficient of determination; p-value: probability of obtaining; T: temperature; C: concentration; t: exposure time.

current and thus the dissolution of metal. The reaction at the metal surface requires a small activation energy and activation enthalpy to proceed if the acid solution concentration is increased. The positive sign for both E_{act} and ΔH_{act} reflects the endothermic nature of the corrosion process while the increase of ΔS_{act} implies an increase in disordering takes place on going from reactants to the activated complex (Go et al., 2020; Okewale and Adesina, 2020). These observations on kinetic parameters of activation corrosion support the PDP and EIS results.

5.5. pH results

The final pH after the experiments is plotted against temperature (Figure 8). The final pH decreases as the temperature increases to 60 °C. With L-ascorbic acid instead of acetic acid, the pH decreases even more to 2.5 at 60 °C. This decrease in pH values if the temperature increases implies the increase in corrosion current densities as confirmed in Tables 3 and 4 (PDP results). Further, the change in concentration from 0.2 to 1.0 mM of either acetic or L-ascorbic acid decreases the pH values and consequently increases the corrosion current densities too. The decrease in L-ascorbic acid is more than in acetic which implies higher corrosion current densities.

5.6. ICP-OES results

The ICP-OES results on dissolved metal ions in solution are shown in Figure 9. The general trend observed is that the concentration of metal ions (Fe, Si, and Mn) in solution increases as temperature and concentration of the organic acid metabolite increase. This trend is consistent with the trend of corrosion current densities. The increase in metal ions into solution when temperature or concentration increases relates to the increase in H^+ and decrease in pH).

According to Madirisha et al. (2022), the ICP-OES results of carbon steel corrosion under SRB conditions, with biofilm and in brine solution show an average concentration of Fe, Si, and Mn of 220 μg/gcm^2 (at 60 and 120 min). Carbon steel corrosion under the same conditions, with the addition of acetic acid (60 and 120 min), in both concentrations (0.2 and 1.0 mM), results in a decrease of the dissolved ion concentration to 60 μg/gcm^2 for 0.2 mM and 170 μg/gcm^2 for 1.0 mM. The addition of L-ascorbic (1.0 mM) instead of acetic acid increases the dissolution of the carbon steel coupon even more to dissolved ion (Fe, Si, and Mn) concentrations of 800 μg/gcm^2 and 1100 μg/gcm^2, at 60 min and 120 min exposure time, respectively. These results further support the PDP and EIS on inhibition and acceleration of corrosion demonstrated by acetic and L-ascorbic acids in a simulated SRB environment, respectively.

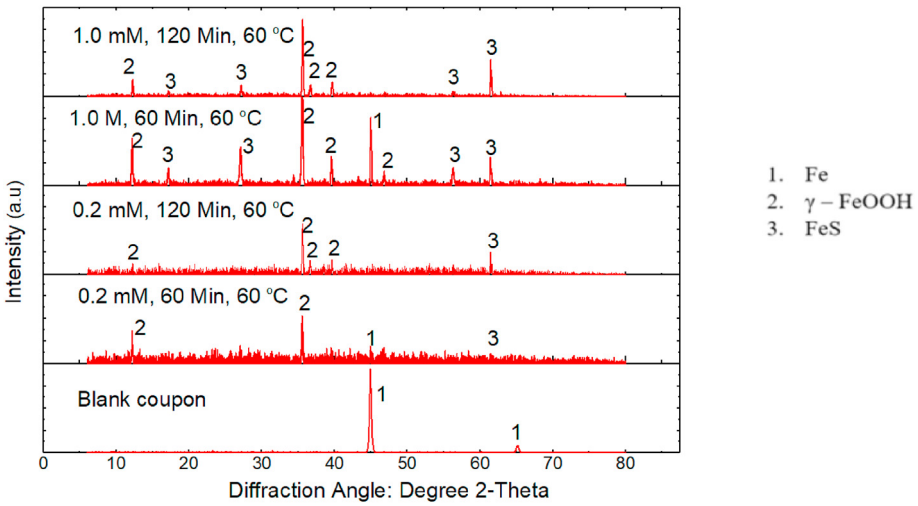

Figure 10. XRD patterns for test coupons in a brine solution with acetic acid as a function of exposure time at 60 °C.

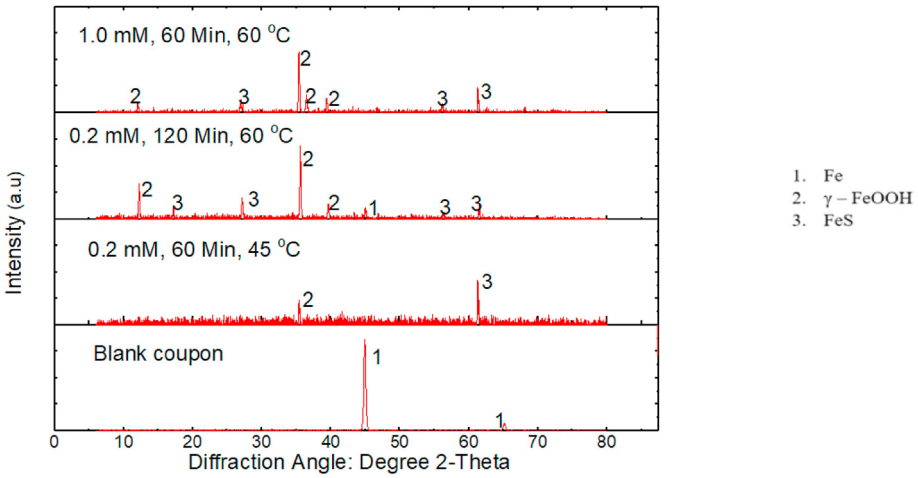

Figure 11. XRD patterns for test coupons in a brine solution with L-ascorbic acid as a function of exposure time and temperature.

5.7. Multiple linear regression

The data shown in Table 8 is analyzed by multiple linear regression to predict the i_{corr} as a function of temperature, exposure time, the concentration of acids, and pH of the solution. The data in Table 8 do not show any quadratic, polynomial, exponential, or logarithmic relation due to near-collinearity among model terms. The R^2, p, and coefficient values are shown in Table 9. The R^2 values show a strong correlation between the variables (0.992 and 0.970). The concentration of acids, temperature, exposure time, and pH have a high influence on the corrosion current densities in either acetic or L-ascorbic acid. The p-value in acetic or L-ascorbic shows a significant correlation because it is less than the statistical accepted value which is 0.05. On the other hand, the coefficient values of independent variables show that the concentration of acid has more influence on corrosion current densities than on pH, temperature, and exposure time. The influence of the concentration of acid on corrosion current densities is more pronounced in L-ascorbic than acetic experiments which in turn implies higher corrosion current densities in the presence of L-ascorbic. These regression results strongly support the PDP, EIS, and pH measurement results.

5.8. XRD results

XRD diffractograms of test coupons corroded in presence of acetic and L-ascorbic acid are shown in Figures 10 and 11, respectively. All coupons have been measured, however only the diffractograms with the most significant alterations are shown. The XRD reveals the occurrence of corrosion products namely FeS and γ-FeOOH in the presence of acetic or L-ascorbic acid in a simulated SRB environment. The presence of these corrosion products under a simulated SRB environment is in agreement with the literature that when SRB are present in the environment, the first corrosion products are ferric (oxyhydroxide) such as lepidocrocite, transformed to the iron sulphide by hydrogen sulphide, chemical Eq. (12) (El Hajj et al., 2013). The presence of corrosion products on test coupons in the presence of acetic or L-ascorbic acid in a simulated SRB environment further supports the occurrence of deterioration on the test coupons.

$$3H_2S + 2FeOOH \rightarrow 2FeS + S + 4H_2O \quad (12)$$

6. Conclusions

The role of simulated organic acid metabolites, namely acetic and L-ascorbic acids on corrosion of geo-energy pipeline made of carbon steel in the presence of simulated Sulfate Reducing Bacteria (SRB) is investigated at different temperatures (30, 45, and 60 °C) and exposure times (60 and 120 min). Abiotic sulfide, CO_2, calcium alginate and NaCl brine are used to simulate the SRB environment. The electrochemical results show that acetic and L-ascorbic acids in a simulated SRB environment accelerate corrosion. Further, the electrochemical weight loss increases with the increase in temperature and concentration of the acetic/L-ascorbic acid which in turn implies an increase in corrosion current densities. These observations are further supported by the kinetic corrosion activation parameters which show an endothermic nature of the corrosion process characterized with a small activation energy and activation enthalpy to proceed if the acid solution concentration is increased. The R^2 from multiple linear regression of corrosion current densities shows that concentration of acids, temperature, exposure time, and pH have a high influence on the corrosion current densities. The p-values in acetic or L-ascorbic show a significant correlation of the variables on corrosion because p-values are less than the statistical accepted value which is 0.05. On the other hand, the coefficient values in the presence of L-ascorbic acid are higher than in acetic acid implying higher corrosion current densities. Furthermore, the ICP-OES shows that the dissolution of metal ions in solution is more in the presence of L-ascorbic than in the presence of acetic acid. The increase of dissolution of carbon steel is accompanied by the decrease of the pH solution when acetic acid and L-ascorbic acid are added. The XRD results also confirm the occurrence of corrosion in the presence of acetic/L-ascorbic acid. This is evidenced by the formation of FeS and γ-FeOOH.

Comparison of electrochemical results in this study with the results in a simulated SRB environment without acetic or L-ascorbic acid shows that the corrosion current densities in the presence of acetic acids in a SRB environment are two times lower than those in a simulated SRB environment without acetic acid under similar experimental conditions (Madirisha et al., 2022). This observation shows that acetic acid in the presence of a simulated SRB environment demonstrates an inhibitory effect. On the other hand, the corrosion current densities in the presence of L-ascorbic acid in a simulated SRB environment are approximately two times higher than without L-ascorbic acid implying that L-ascorbic acid accelerates corrosion. The effect on corrosion current densities demonstrated by acetic and L-ascorbic acids in a simulated SRB environment is not found in the literature. Furthermore, the ICP-OES results support the corrosion inhibitory and acceleration effects due to the presence of acetic and L-ascorbic acid, respectively. Taking into account the ICP-OES results (average concentration of Fe, Si, and Mn is 220 ug/gcm^2) of test coupons under SRB conditions without acetic or L-ascorbic acid reported in Madirisha et al. (2022), adding acetic acid with concentrations 0.2 and 1.0 mM (60 and 120 min), decreases the dissolved metal ion concentration to 60 μg/gcm^2 for 0.2 mM and 170 μg/gcm^2 for 1.0 mM. The addition of L-ascorbic (1M) instead of acetic acid increases the dissolution of the carbon steel test coupons even more to dissolved ion (Fe, Si,

and Mn) concentrations of 800 μg/gcm^2 and 1100 μg/gcm^2, at 60 min and 120 min exposure time, respectively. The results complement the existing literature on the role of acetic and L-ascorbic acids on corrosion of carbon steel in a SRB environment and highlight the novelty of this research. In addition, the results highlight the role of H_2S in organic acid corrosion as being the key role. The results have a direct impact on the role of other microbial metabolites in the corrosion of carbon steel.

Declarations

Author contribution statement

Makungu Madirisha: Conceived and designed the experiments; Performed the experiments; Analyzed and interpreted the data; Wrote the paper.

Robert Hack, Freek van der Meer: Conceived and designed the experiments; Analyzed and interpreted the data; Contributed reagents, materials, analysis tools or data; Wrote the paper.

Funding statement

This work was supported by The Netherlands Initiative for Capacity Development in Higher Education, NICHE-NUFFIC through the Tanzania – Dutch Energy Capacity Building project, TDECB (OFI93936314).

Data availability statement

Data included in article/supplementary material/referenced in article.

Declaration of interests statement

The authors declare no conflict of interest.

Additional information

No additional information is available for this paper.

Acknowledgements

The Nelson Mandela Institute of Science and Technology, Arusha, Tanzania is acknowledged for allowing to use of their laboratory and electrochemical facilities. The Geoscience laboratory of the Faculty of Geo-Information Science and Earth Observation, University of Twente is acknowledged for the ICP-OES and XRD analyses. Further, The Tanzania Petroleum Development Corporation (TPDC) is acknowledged for providing the carbon steel API 5L X70M HFW.

References

Abadeh, H.K., Javidi, M., 2019. Assessment and influence of temperature, NaCl and H2S on CO2 corrosion behavior of different microstructures of API 5L X52 carbon steel in aqueous environments. J. Nat. Gas Sci. Eng. 67, 93–107.

Ahmad, Z., 2006. Institution of chemical engineers (Great Britain). In: Principles of Corrosion Engineering and Corrosion Control. Elsevier/BH, Boston, MA.

Alabbas, F.M., Mishra, B., 2013. Microbiologically influenced corrosion of pipelines in the oil & gas industry. In: Proceedings of the 8th Pacific Rim International Congress on Advanced Materials and Processing. Springer, pp. 3441–3448.

Almela, P., Justel, A., Quesada, A., 2021. Heterogeneity of microbial communities in soils from the antarctic peninsula region. Front. Microbiol. 12, 628792.

Amri, J., Gulbrandsen, E., Nogueira, R.P., 2011. Role of Acetic Acid in CO2 Top of the Line Corrosion of Carbon Steel. NACE - International Corrosion Conference Series, Houston - USA.

Apostolopoulos, C.A., Demis, S., Papadakis, V.G., 2013. Chloride-induced corrosion of steel reinforcement–Mechanical performance and pit depth analysis. Construct. Build. Mater. 38, 139–146.

Audiffrin, C., Cayol, J.-L., Joulian, C., Casalot, L., Thomas, P., Garcia, J.-L., Ollivier, B., 2003. Desulfonauticus submarinus gen. nov., sp. nov., a novel sulfate-reducing bacterium isolated from a deep-sea hydrothermal vent. Int. J. Syst. Evol. Microbiol. 53, 1585–1590.

Bao, Q., Zhang, D., Lv, D., Wang, P., 2012. Effects of two main metabolites of sulphate-reducing bacteria on the corrosion of Q235 steels in 3.5wt.% NaCl media. Corrosion Sci. 65, 405–413.

Blackwood, D., 2018. An electrochemist perspective of microbiologically influenced corrosion. Corrosion and Materials Degradation 1, 59–76.

Bonis, M., Crolet, J., 1989. Basics of the Prediction of the Risks of CO2 Corrosion in Oil and Gas Wells||, Paper No. 466. Corrosion/89, April, 17-21.

Caneva, G., Nugari, M.P., Salvadori, O., 2008. Plant Biology for Cultural Heritage: Biodeterioration and Conservation. Getty Publications.

Chang, X., Chen, S., Yin, C., Cheng, S., Liu, T., Yin, Y., 2010. Study of Fe3Al corrosion behavior in simulating marine biofilm environment. Mater. Manuf. Process. 25, 302–306.

Chidiebere, M.A., Oguzie, E.E., Liu, L., Li, Y., Wang, F., 2015. Ascorbic acid as corrosion inhibitor for Q235 mild steel in acidic environments. J. Ind. Eng. Chem. 26, 182–192.

Clarke, B.H., Aguilera, A.M., 2001. Microbiologically influenced corrosion in fire sprinkler systems. Fire Protect. Eng. 9, 14–22.

Cramer, S.D., Covino, B.S., 2003. ASM Handbook: Corrosion: Fundamentals, Testing, and protection, vol. 13 A. ASM International.

Crolet, J., Bonis, M., 1983. pH measurements in aqueous CO2 solutions under high pressure and temperature. Corrosion 39, 39–46.

Dariva, C.G., Galio, A.F., 2014. Corrosion inhibitors-principles , mechanisms and applications. In: Developments in Corrosion Protection. IntechOpen, pp. 365–378.

Davis, K.M., Isberg, R.R., 2016. Defining heterogeneity within bacterial populations via single cell approaches. Bioessays 38, 782–790.

Dresel, P., Rose, A., 2010. Chemistry and Origin of Oil and Gas Well Brines in Western Pennsylvania, Open-File Oil and Gas Report 10-01.0. Pennsylvania geological survey.

El Hajj, H., Abdelouas, A., El Mendili, Y., Karakurt, G., Grambow, B., Martin, C., 2013. Corrosion of carbon steel under sequential aerobic–anaerobic environmental conditions. Corrosion Sci. 76, 432–440.

Ferreira, E., Giacomelli, C., Giacomelli, F., Spinelli, A., 2004. Evaluation of the inhibitor effect of L-ascorbic acid on the corrosion of mild steel. Mater. Chem. Phys. 83, 129–134.

Fuadi, A., 2019. Investigation of ascorbic acid as environment-friendly corrosion inhibitor of low carbon steel in marine environment. In: IOP Conference Series: Materials Science and Engineering, vol. 536. IOP Publishing, p. 12108.

Fuchs-Godec, R., Pavlović, M., Tomić, M.V., 2013. The inhibitive effect of vitamin-C on the corrosive performance of steel in HCl solutions. Int. J. Electrochem. Sci. 8, 1551-1519.

Go, L.C., Depan, D., Holmes, W.E., Gallo, A., Knierim, K., Bertrand, T., Hernandez, R., 2020. Kinetic and thermodynamic analyses of the corrosion inhibition of synthetic extracellular polymeric substances. PeerJ Mater. Sci. 2, e4.

Gu, T., Jia, R., Unsal, T., Xu, D., 2019. Toward a better understanding of microbiologically influenced corrosion caused by sulfate reducing bacteria. J. Mater. Sci. Technol. 35, 631–636.

Hong, M.-S., Kim, S.-H., Im, S.-Y., Kim, J.-G., 2016. Effect of ascorbic acid on the pitting resistance of 316L stainless steel in synthetic tap water. Met. Mater. Int. 22, 621–629.

Hussain, A., Hasan, A., Javid, A., Qazi, J.I., 2016. Exploited application of sulfate-reducing bacteria for concomitant treatment of metallic and non-metallic wastes: a mini review. 3 Biotech 6, 119.

Ibrahim, A., Hawboldt, K., Bottaro, C., Khan, F., 2018. Review and analysis of microbiologically influenced corrosion: the chemical environment in oil and gas facilities. Corrosion Eng. Sci. Technol. 53, 549–563.

Jia, R., Tan, J.L., Jin, P., Blackwood, D.J., Xu, D., Gu, T., 2018. Effects of biogenic H2S on the microbiologically influenced corrosion of C1018 carbon steel by sulfate reducing Desulfovibrio vulgaris biofilm. Corrosion Sci. 130, 1–11.

Jia, R., Yang, D., Al-Mahamedh, H.H., Gu, T., 2017. Electrochemical testing of biocide enhancement by a mixture of D-amino acids for the prevention of a corrosive biofilm consortium on carbon steel. Ind. Eng. Chem. Res. 56, 7640–7649.

Kahyarian, A., Schumaker, A., Brown, B., Nesic, S., 2017. Acidic corrosion of mild steel in the presence of acetic acid: mechanism and prediction. Electrochim. Acta 258, 639–652.

Khadom, A.A., Yaro, A.S., AlTaie, A., Kadum, A., 2009. Electrochemical, activations and adsorption studies for the corrosion inhibition of low carbon steel in acidic media. Port. Electrochim. Acta 27, 699–712.

Kiani Khouzani, M., Bahrami, A., Hosseini-Abari, A., Khandouzi, M., Taheri, P., 2019. Microbiologically influenced corrosion of a pipeline in a petrochemical plant. Metals 9, 459.

Kim, M., Cho, A., Lim, H.S., Hong, S.G., Kim, J.H., Lee, J., Choi, T., Ahn, T.S., Kim, O.-S., 2015. Highly heterogeneous soil bacterial communities around Terra Nova Bay of northern Victoria Land, Antarctica. PLoS One 10, e0119966.

Kushkevych, I., Hýžová, B., Vítězová, M., Rittmann, S.K.-M., 2021. Microscopic methods for identification of sulfate-reducing bacteria from various habitats. Int. J. Mol. Sci. 22, 4007.

Li, H., Xu, D., Li, Y., Feng, H., Liu, Z., Li, X., Gu, T., Yang, K., 2015. Extracellular electron transfer is a bottleneck in the microbiologically influenced corrosion of C1018 carbon steel by the biofilm of sulfate-reducing bacterium Desulfovibrio vulgaris. PLoS One 10, e0136183.

Li, S.-L., Wang, Y.-J., Chen, Y.-C., Liu, S.-M., Yu, C.-P., 2019. Chemical characteristics of electron shuttles affect extracellular electron transfer: shewanella decolorationis NTOU1 simultaneously exploiting acetate and mediators. Front. Microbiol. 10, 399.

Li, Y., Ning, C., 2019. Latest research progress of marine microbiological corrosion and bio-fouling, and new approaches of marine anti-corrosion and anti-fouling. Bioact. Mater. 4, 189–195.

Li, Y., Xu, D., Chen, C., Li, X., Jia, R., Zhang, D., Sand, W., Wang, F., Gu, T., 2018. Anaerobic microbiologically influenced corrosion mechanisms interpreted using bioenergetics and bioelectrochemistry: a review. J. Mater. Sci. Technol. 34, 1713–1718.

Little, B., Blackwood, D., Hinks, J., Lauro, F., Marsili, E., Okamoto, A., Rice, S., Wade, S., Flemming, H.-C., 2020. Microbially influenced corrosion–any progress? Corrosion Sci. 170, 108641.

Little, B.J., Lee, J.S., Ray, R., 2006. Diagnosing microbiologically influenced corrosion: a state-of-the-art review. Corrosion 62, 1006–1017.
Lugauskas, A., Prosycevas, I., Ramanauskas, R., Asta Griguceviciene, A., Selskiene, A., Pakštas, V., 2009. The Influence of Micromycetes on the Corrosion Behaviour of Metals (Steelal) under conditions of the environment polluted with organic substances. Medziagotyra 15, 224–235.
Madirisha, M., Hack, R., van der Meer, F., 2022. Simulated microbial corrosion in oil, gas and non-volcanic geothermal energy installations: the role of biofilm on pipeline corrosion. Energy Rep. 8, 2964–2975.
Magot, M., Ollivier, B., Patel, B.K., 2000. Microbiology of petroleum reservoirs. Antonie Leeuwenhoek 77, 103–116.
Magot, M., Tardy-Jacquenod, C., Crolet, J.-L., 1997. An Updated Portrait of the Sulfidogenic Bacteria Potentially Involved in the Microbial Corrosion of Steel, vol. 686. Book-Institute of Materials, pp. 3–10.
Munoz, A., Andrade, C., Torres, A., 2007. Corrosion products pressure needed to crack the concrete cover. Adv. Constr. Mater. 2007, 359–370.
Muramatsu, Y., Komatsu, R., Sawaki, T., Sasaki, M., Yanagiya, S., 2000. Geochemical study of fluid inclusions in anhydrite from the Kakkonda geothermal system, northeast Japan. Geochem. J. 34, 175–193.
Naranjo, L., Pernía, B., Inojosa, Y., Rojas, D., D'Anna, L.S., González, M., Sisto, Á.D., 2015. First evidence of fungal strains isolated and identified from naphtha storage tanks and transporting pipelines in Venezuelan oil facilities. Adv. Microbiol. 5, 143–154.
Nassif, L.A., Rioual, S., Farah, W., Hellio, C., Fauchon, M., Trepos, R., Abboud, M., Diler, E., Thierry, D., Lescop, B., 2020. Reduction of potential ennoblement of stainless steel in natural seawater by an ecofriendly biopolymer. J. Environ. Chem. Eng. 8, 103609.
Nogara, J., Zarrouk, S.J., 2018. Corrosion in geothermal environment Part 2: metals and alloys. Renew. Sustain. Energy Rev. 82, 1347–1363.
Okewale, A., Adesina, O., 2020. Kinetics and thermodynamic study of corrosion inhibition of mild steel in 1.5 M HCl medium using cocoa leaf extract as inhibitor. J. Appl. Sci. Environ. Manag. 24, 37–47.
Parthipan, P., Elumalai, P., Karthikeyan, O.P., Ting, Y.P., Rajasekar, A., 2017. A review on biodegradation of hydrocarbon and their influence on corrosion of carbon steel with special reference to petroleum industry. J. Environ. Biotechnol. Res. 6, 12–33.
Plugge, C., Zhang, W., Scholten, J., Stams, A., 2011. Metabolic flexibility of sulfate-reducing bacteria. Front. Microbiol. 2, 81.
Popoola, L.T., Grema, A.S., Latinwo, G.K., Gutti, B., Balogun, A.S., 2013. Corrosion problems during oil and gas production and its mitigation. Int. J. Integrated Care 4, 35.
Provoost, M., Albeda, L., Godschalk, B., van der Werff, B., Schoof, F., 2018. Geothermal energy use, country update for The Netherlands. Policy 2015 (3.1).
Reinecker, J., Hochschild, T., Kraml, M., Löschan, G., Kreuter, H., 2019. Experiences and challenges in geothermal exploration in the Upper Rhine Graben. In: Proceedings of European Geothermal Congress, pp. 11–12.
Riskin, J., Khentov, A., 2019. Electrocorrosion and protection of Metals. Elsevier.
Sanchez, J., Fullea, J., Andrade, C., 2017. Corrosion-induced brittle failure in reinforcing steel. Theor. Appl. Fract. Mech. 92, 229–232.
Sand, W., Gehrke, T., 2003. Microbially influenced corrosion of steel in aqueous environments. Rev. Environ. Sci. Biotechnol. 2, 169–176.
Singh, M., Gupta, A., 2000. Corrosion behavior of mild steel in acetic acid solutions. Corrosion 56, 371–379.
Singh, S., Mukherjee, A., 2010. Kinetics of mild steel corrosion in aqueous acetic acid solutions. J. Mater. Sci. Technol. 26, 264–269.
Streicher, M., 2011. In: Revie, R.W. (Ed.), Uhlig's Corrosion Handbook, third ed. John Wiley & Sons, Hoboken, NJ.
Tran, T.T.T., Kannoorpatti, K., Padovan, A., Thennadil, S., 2021. Sulphate-reducing bacteria's response to extreme pH environments and the effect of their activities on microbial corrosion. Appl. Sci. 11, 2201.
Videla, H.A., Herrera, L.K., 2009. Understanding microbial inhibition of corrosion. A comprehensive overview. Int. Biodeterior. Biodegrad. 63, 896–900.
Wang, D., Liu, J., Jia, R., Dou, W., Kumseranee, S., Punpruk, S., Li, X., Gu, T., 2020. Distinguishing two different microbiologically influenced corrosion (MIC) mechanisms using an electron mediator and hydrogen evolution detection. Corrosion Sci. 177, 108993.
Wang, J., Meng, L., Fan, Z., Liu, Q., Tong, Z., 2019. Mechanism and Modelling of CO2 Corrosion on Downhole Tools, vol. 6. Royal Society Open Science, p. 181899.
Wolf, P.G., Biswas, A., Morales, S.E., Greening, C., Gaskins, H.R., 2016. H2 metabolism is widespread and diverse among human colonic microbes. Gut Microb. 7, 235–245.
Wong, G.C., Antani, J.D., Lele, P.P., Chen, J., Nan, B., Kühn, M.J., Persat, A., Bru, J.-L., Høyland-Kroghsbo, N.M., Siryaporn, A., 2021. Roadmap on emerging concepts in the physical biology of bacterial biofilms: from surface sensing to community formation. Phys. Biol. 18, 051501.
Xu, D., Li, Y., Gu, T., 2016. Mechanistic modeling of biocorrosion caused by biofilms of sulfate reducing bacteria and acid producing bacteria. Bioelectrochemistry 110, 52–58.
Zuo, R., 2007. Biofilms: strategies for metal corrosion inhibition employing microorganisms. Appl. Microbiol. Biotechnol. 76, 1245–1253.